Effect of shock subs on self-excited vibrations in drilling systems

Please check the document version of this publication:

• A submitted manuscript is the version of the article upon submission and before peer-review. There can be important differences between the submitted version and the official published version of record. People interested in the research are advised to contact the author for the final version of the publication, or visit the DOI to the publisher's website.
• The final author version and the galley proof are versions of the publication after peer review.
• The final published version features the final layout of the paper including the volume, issue and page numbers.

[Link to publication](#)

Effect of shock subs on self-excited vibrations in drilling systems

Ulf Jakob F. Aarsnes[a,*], Nathan van de Wouw[b,c]

[a] Norwegian Research Centre AS, Oslo, Norway
[b] Eindhoven University of Technology, Department of Mechanical Engineering, Eindhoven, the Netherlands
[c] Department of Civil, Environmental & Geo-Engineering, University of Minnesota, Minneapolis, USA

ABSTRACT

The present paper studies the effect of an axial elastic tool (known as a shock sub), mounted downhole in the drill-string, on the occurrence of axial and torsional self-excited vibrations. In particular, we evaluate the feasibility of stabilizing the axial dynamics, dominated by a bilateral (feedback) coupling between the bit-rock interaction and the drill-string wave-equations, through the insertion of a passive down-hole tool. We consider the problem of unwanted drill-string vibrations and explain how these vibrations relate to the so-called axial instability using a distributed parameter (infinite dimensional) model. The equations describing the feedback system causing this instability are derived and then extended to accommodate for the inclusion of the effect of the shock sub. Conditions for the design parameters of the shock sub needed to avoid axial instability are then derived and their practical feasibility are considered.

1. Introduction

Rotary drilling systems are often plagued by the phenomenon known as self-excited vibrations. The occurrence of self-excited vibrations coincides with the existence of one or more unstable modes in the model describing the system dynamics. The implications of an unstable mode is that a small initial perturbation will grow over time until it manifests itself as oscillations, which in severe cases can be observed as stick-slip or bit bouncing vibrations. Such severe vibrations can decrease drilling performance and cause premature equipment wear and increased non-productive time (Jardine et al., 1994; Ghasemloonia et al., 2015). The present study will be concerned with fixed cutter bits (also known as PDC bits) as these are the most popular bit type used in the industry and are especially prone to self-excited vibrations.

Torsional stick-slip refers to the case where the bits angular velocity becomes temporarily stationary during the oscillation, as caused by an unstable torsional mode. The unstable torsional mode is often modeled as caused by a rate-weakening effect (Dunayevsky and Abbassian, 1998), and while drill string side forces clearly can display such behavior (Aarsnes and Shor, 2018a; Aarsnes et al., 2019), there is no intrinsic rate weakening effect in the bit-rock interaction (Nishimatsu, 1972). However, even a rate-independent bit-rock interaction can cause self excited vibrations (Richard et al., 2007) through the regenerative effect (Insperger et al., 2006) which have been throughly studied in the field for metal machining (Tobias, 1965; Kalmár-Nagy et al., 2001).

Although the rate-weakening of side forces and the regenerative bit-rock interaction are distinct phenomena, these can both lead to stick slip (Aarsnes and Shor, 2018b). We will in this paper focus on the regenerative effect in the bit-rock interaction as a cause of vibrations.

It has been shown that there are two (coupled) loops capable of causing instability, a loop involving the torsional dynamics and a loop involving the axial dynamics (Aarsnes and Aamo, 2016). While the torsional loop might be stabilizable from the top-drive (Kyllingstad and Nessjøen, 2009; Runia et al., 2013; Dwars, 2015; Besselink et al., 2016; Vromen et al., 2017a, 2017b), the axial instability is in most cases too severe for this to be a feasible approach (Aarsnes and van de Wouw, 2018). Furthermore, it has been proposed that torsional stick-slip oscillations might be a consequence of the axial instability (Richard et al., 2007; Germay et al., 2009a; Besselink et al., 2011); specifically in (Germay et al., 2009a) it is stated that "the apparent decrease of the mean torque with the angular velocity responsible for the growth of the amplitude of the torsional vibrations is a consequence of the axial vibrations.", however, this explanation was not directly replicated with a distributed drill-string model in (Aarsnes and van de Wouw, 2019), where instead it was indicated that a high axial loop gain (associated with axial instability) has a stabilizing effect on the torsional dynamics, and that the presence of axial instability can increase ROP. A similar conclusion was drawn in (Gupta and Wahi, 2018).

However, it remains of significant interest to evaluate approaches to manipulate the stability of the axial loop of the bit-rock–drill-string

---

system, for the following reasons:

1. If the rate-weakening effect causing the torsional stick-slip oscillations is caused by the axial limit-cycle, then by avoiding the axial instability torsional stick-slip oscillations are also avoided. The possibility of such an approach is mentioned in (Besselink et al., 2011, 2016; Yigit and Christoforou, 2006) but an actual solution has not yet been presented.

2. A recent avenue of research is on the effect of axial instability on the relation between WOB and ROP, where it has been proposed that an axial limit cycle can increase ROP for a given averaged weigh-on-bit (Aarsnes and van de Wouw, 2019; van de Wouw et al., 2017).

The present paper investigates the effect of inserting a down-hole tool (shock sub) in the drill-string, with the appropriate axial dynamics (frequency response characteristics), on the axial and torsional stability of bit-rock–drill-string feedback system. BHA redesign has been used to reduce lateral vibrations (Bailey and Remmert, 2010), and we expect that improvement can be achieved for torsional and axial vibrations as well. The analysis does not include the effect of interaction between the drill-string and the borehole. Still, we argue that this approximation is a reasonable first step in investigating the effect of shock subs on self-excited vibrations. This paper is to our knowledge the first stability analysis presented in the literature of a drill string with an elastic tool and the bit-rock interaction as in (Richard et al., 2007).

This work builds on the developments in (Aarsnes and Aamo, 2016) and (Aarsnes and van de Wouw, 2018), where the bit-rock interaction proposed in (Richard et al., 2007) is used with a distributed (infinite-dimensional) description of the drill-string dynamics to arrive at a frequency-domain stability analysis result. The main novel contributions of the current paper are as follows. Firstly, the use of a down-hole tool (i.e., a shock sub) is proposed to manipulate the axial drill-string dynamics. Secondly, a local stability analysis of the resulting dynamics is performed, culminating in conclusions on the potential for such a down-hole tool to manipulate or eliminate the axial instability and therewith, potentially, the root cause for torsional stick-slip oscillations. Finally, the implementation of such an elastic tool in a non-linear simulation model is pursued which verifies the stability conclusions of the local analysis.

The structure of the paper is as follows. The model of the drill-string and the bit–rock interaction is described in Appendix A, which also includes the corresponding frequency-domain model description. This model, which is described in Appendix A and concisely recapped in Section 2.1, is used to derive the system's stability criteria to be employed in the following section. Then, in Section 3, we modify the model and its transfer functions to incorporate the effect of the elastic tool, and conditions on its design and placement to ensure stability are derived. Finally, in Section 4, a time-domain implementation of the model is simulated which confirms the conclusions from the frequency-domain analysis.

2. Stability analysis

In this section, we briefly recap the drill-string stability conditions as stated in (Aarsnes and van de Wouw, 2018). The transfer functions used for stability analysis are derived in Appendix A. A nomenclature of the symbols used is given in Table 1.

2.1. Frequency-domain model description

The Laplace transformed variables are indicated by capital letters, with the independent parameter $s \in \mathbb{C}$ denoting the Laplace variable. For the axial dynamics, $g_a(s)$ relates weight on bit W_b to axial bit velocity V_b as follows: The drill string transfer functions are

Table 1
Nomenclature.

Independent variables	
S	Laplace variable
T	Time in seconds
x	Axial position in meters
Independent variables	
w	Force
τ	Torque
v	Axial velocity
ω	Angular velocity
Laplace transformed states $i \in \{0, p, s, b\}$ denotes 'top-drive', 'pipe bottom', 'collar top' and 'bit', respectively.	
W_i	Weight
T_i	Torque
V_i	Axial velocity
Ω_i	Angular velocity
Derived quantities, for $i \in \{a, t\}$ (axial, torsional) and $j \in \{p, c\}$ (pipe, collar).	
$t_N = \frac{\bar{v}}{N\bar{\omega}}$	Steady-state BRI delay
$\zeta_i^p = \frac{A^j E}{c_a}, \frac{J^j G}{c_t}$	Axial/torsional impedance
$c_i = \sqrt{\frac{E}{\rho}}, \sqrt{\frac{G}{\rho}}$	Axial/torsional, wave speed
$t_i^j = \frac{L^j}{c_i}$	Axial/torsional travel time
$K_a = \frac{a\zeta \varepsilon N}{\zeta_a^j}$	Nominal axial loop gain
$K_t = \frac{\bar{v}}{\bar{\omega}} \frac{a^2 \varepsilon N}{2\zeta_t^j}$	Nominal torsional loop gain
$M_b = A_c \rho L_c$	Mass of collar section
Transfer functions	
$Z_i^j(s) = \zeta_i^j \left(1 + \frac{k_i}{s}\right)^{1/2}$	
$Z_i^L(s) = -\frac{W_0}{V_0}(s), -\frac{T_0}{\Omega_0}(s)$	
$\Gamma_i^j(s) = st_i^j \left(1 + \frac{k_i}{s}\right)^{1/2}$	
$g_i(s) = -\zeta_a \frac{V_b}{W_b}, -\zeta_t \frac{\Omega_b}{T_b}$	
$D(s) = \frac{N}{s}\left[V_b(s)(1 - e^{-t_N s}) - \frac{\bar{v}}{\bar{\omega}}\Omega_b(s)(1 - e^{-t_N s})\right]$	
$G(s) = G_a(s) + G_t(s)$	

Table 2
Parameter values.

$a = 0.108$	[m]		Bit cutter radius
$\varepsilon = 20 \times 10^6$	[Pa]		Rock specific energy
$\zeta = 0.6$	[-]		Bit cutter angle
$N = 4$	[-]		Number of cutters
$A_p = 0.0035$	[m^2]		Drill-string area
$A_c = 0.0209$	[m^2]		Drill collar area
$J_p = 1.22 \times 10^{-5}$	[m^4]		Drill-string polar inertia
$J_c = 5.19 \times 10^{-5}$	[m^4]		Drill collar polar inertia
$L_p = 1000$	[m]		Drill-string length
$L_c = 300$	[m]		Drill collar length
$E = 200 \times 10^9$	[Pa]		Youngs modulus
$G = 77 \times 10^9$	[m]		Shear modulus
$\rho = 8000$	[kg/m^3]		Density
$k_a = 0.3$	[-]		Axial domain damping
$k_t = 0.3$	[-]		Torsional domain damping
$V_0 = 30$	[m/h]		Top drive axial velocity
$\omega_0 = 61.5$	[RPM]		Top drive angular velocity

$$\frac{V_b}{W_b}(s) = -\frac{1}{\zeta_a}g_a(s), \quad g_a(s) := \frac{\zeta_a \, Z_a^i + Z_a^L \tanh \Gamma_a}{Z_a^i \, Z_a^L + Z_a^i \tanh \Gamma_a}, \tag{1}$$

$$\frac{\Omega_b}{T_b}(s) = -\frac{1}{\zeta_t}g_t(s), \quad g_t(s) := \frac{\zeta_t \, Z_t^i + Z_t^L \tanh \Gamma_t}{Z_t \, Z_t^L + Z_t^i \tanh \Gamma_t}, \tag{2}$$

where

$$Z_a^i(s) = \zeta_a^i \left(1 + \frac{k_a}{\rho s}\right)^{1/2}, \quad \Gamma_a^i(s) = st_a^i \left(1 + \frac{k_a}{\rho s}\right)^{1/2}, \tag{3}$$

$$Z_t^i(s) = \zeta_t^i \left(1 + \frac{k_t}{\rho s}\right)^{1/2}, \quad \Gamma_t^i(s) = st_t^i \left(1 + \frac{k_t}{\rho s}\right)^{1/2}, \tag{4}$$

with $\quad \zeta_a^i := \frac{A_i E}{c_a}, \quad t_a^i := \frac{L_i}{c_a}, \quad \zeta_t^i := \frac{J_i G}{c_t}, \quad t_t^i := \frac{L_i}{c_t}, \quad i \in \{p, c\}, \quad$ and $c_a = \sqrt{E/\rho}$, $c_t = \sqrt{G/\rho}$, while the load impedances $Z_t^L(s) := \frac{T_0}{\Omega_0}(s)$, $Z_a^L(s) := \frac{W_0}{V_0}(s)$ depend on the boundary conditions.

The linearized bit-rock interaction in the frequency-domain is

$$W_b(s) = a\zeta\varepsilon D(s), \quad T_b(s) = \frac{1}{2}a^2\varepsilon D(s), \tag{5}$$

and

$$D(s) = \frac{N}{s}\left[V_b(s)\left(1 - e^{-t_N s}\right) - \frac{\bar{v}}{\omega_0}\Omega_b(s)\left(1 - e^{-t_N s}\right)\right]. \tag{6}$$

2.2. Stability criteria

The stability can be determined from the characteristic equation, found by combining (1), (2), (5), (6),

$$G(s) + 1 = 0, \qquad G(s) = G_a(s) + G_t(s), \tag{7}$$

where

$$G_a(s) = g_a(s)\frac{K_a}{s}\left(1 - e^{-st_N}\right), \quad K_a = \frac{a\zeta\varepsilon N}{A_p\sqrt{E\rho}}, \tag{8}$$

$$G_t(s) = -g_t(s)\frac{K_t}{s}\left(1 - e^{-st_N}\right), \quad K_t = \frac{Ra^2\varepsilon N}{2J_p\sqrt{G\rho}}. \tag{9}$$

This characteristic equation can be found by solving for the system of Eqs. (A.12), (A.13), (5), (A.18), and stability can be evaluated by the Nyquist criterion (Aarsnes and Aamo, 2016). We refer to (Aarsnes and van de Wouw, 2018) for a detailed discussion of this result.

2.3. Heuristics for determining stability

A slightly conservative restatement of the stability conditions in (Aarsnes and van de Wouw, 2018) results is the following: If there does not exist a $\omega \in \mathbb{R}$ such that both conditions 1 and 2:

Condition1: $|\arg G(j\omega)| = 180\deg$ \hfill (10)

Condition2: $|G(j\omega)| > 1$, \hfill (11)

are satisfied, then asymptotic stability is guaranteed.

Due to the combination of an axial and a torsional term appearing in (7), evaluating this condition is still challenging. A further simplifying approximation is to evaluate the torsional and the axial loops in isolation, as is proposed in (Aarsnes and van de Wouw, 2018), as this will still yield insight into how and if an instability can be avoided. The reasoning behind this approximation is that, as instabilities will be associated with an axial or torsional resonance of the drill string (Aarsnes and Aamo, 2016), the response of either the axial or torsional term will typically be dominating (in magnitude) the characteristic equation around the frequencies where an instability occurs. Consequently, stabilizing the isolated dynamics of both the torsional and axial loop will tend to stabilize the full system.

For the axial dynamics, we will check the conditions:

ConditionA1: $|\arg G_a(s)| = 180\deg$. \hfill (12)

ConditionA2: $|G_a(s)| > 1$, \hfill (13)

and similarly, for the torsional dynamics we have the conditions:

ConditionB1: $|\arg G_t(s)| = 180\deg$ \hfill (14)

ConditionB2: $|G_t(s)| > 1$. \hfill (15)

2.4. Discussion of the stability result

The Bode diagrams are obtained by evaluating the corresponding transfer function at $s = \frac{j f}{2\pi}$ where $j = \sqrt{-1}$ and f is a vector of frequencies in Hertz. The Bode diagram then shows the magnitude and phase of the complex-valued transfer function.

The torsional and axial terms of the characteristic equation (7) are shown in Figs. 2 and 3, respectively. These terms describe the system dynamics with the parameters shown in Table 2. In these figures, the many repeating resonances of the infinite-dimensional drill string can be observed, as well as relative higher magnitude of the axial term, compared to the torsional, which is typical for drilling systems (Richard et al., 2004; Germay et al., 2009b).

Referring to the Bode diagram of the axial term, shown in Fig. 3, it is clear that (almost) perfect impedance matching ($Z_a^L = Z_a^c$) is required to avoid instabilities. This is infeasible to achieve in practice as it would require actuation of both high frequency and magnitude, although a good impedance matching in a limited frequency range is possibly achievable.

Consider the axial drill-string transfer function $g_a(s)$ of a single section drill-string:

$$g_a(s) = \frac{\zeta_a}{Z_a}\frac{Z_a + Z_a^L \tanh\Gamma_a}{Z_a^L + Z_a \tanh\Gamma_a}. \tag{16}$$

Now, noting that any topside actuation affects the dynamics through the load $Z_{L,a}$ (i.e., this transfer function can be designed within the physical limitations of the actuation system), we can obtain an idea of resulting behavior by considering the extreme cases $Z_{L,a} \to 0$, corresponding to a constant applied hook load, and $Z_{L,a} \to \infty$, corresponding to a constant velocity of the block. We obtain

$$\lim_{|Z_{L,a}|\to\infty} g_a(s) \to \frac{1}{c_a Z_{c,a}}\tanh\Gamma_a \tag{17}$$

$$\lim_{Z_{L,a}\to 0} g_a(s) \to \frac{1}{c_a Z_{c,a}}\frac{1}{\tanh\Gamma_a} \tag{18}$$

$$\lim_{Z_{L,a}\to Z_{c,a}} g_a(s) \to \frac{1}{c_a Z_{c,a}}. \tag{19}$$

The difference between the cases of $Z_{L,a} \to 0$ and $Z_{L,a} \to \infty$ is an inversion of the resonances and anti-resonances, while the final case shows the effect of impedance matching, which yields transfer functions without resonances and anti-resonances. These extreme cases gives a good idea about to what degree the drill string transfer function can be manipulated through the topside boundary condition, as any linear system representation of the topside loads $Z_a^L, Z_t^L \in [0, \infty]$ we would expect to yield a drill string transfer function lying between the two extremes. Resuming, we can say that in practice it is very challenging (if not impossible) to satisfy the stability conditions for the axial dynamics by only surface-based control.

We also note for the axial feedback loop that condition **A1**, in (12), can only be satisfied when $\arg\{1 - e^{-s/\omega_0}\} < 0\deg$ and $\arg g_a < 0\deg$, due to the fact that $\arg\{1 - e^{-s/\omega_0}\}$, $\arg g_a \in [-90,90]\deg$. Combining with criteria **A2**, in (13), the axial term can only cause instability if the gain of the term exceeds unity in the frequency range where the delay term and the axial drill-string transfer functions both have negative phase contributions. To see this, note the phase contribution of the integral factor $\arg 1/s = -90\deg$.

The stability properties of the torsional term is discussed in detail by (Aarsnes and van de Wouw, 2018). Among the conclusions is that the nominal loop gain K_t, of the torsional term $G_t(s)$, typically is smaller than one. This makes impedance matching a feasible approach to avoid instability through avoiding condition **B2** in (15), unlike for the axial term where typically $K_a > 1$.

3. Modeling and analysis of a down-hole elastic tool (shock sub)

In this section, we explore how a shock sub, essentially a down-hole tool with a high elasticity, affects the axial dynamics and, in particular, the stability of the axial loop.

This analysis will be performed in the frequency-domain, and as such, the next section describes the derivation of the necessary transfer functions of a drill string with a down-hole elastic tool. Next, a technique is presented which allows for removing, or calibrating the severity of, the axial instability through the correct placement of the elastic tool.

3.1. Drill-string transfer function

We derive the axial transfer function $g_a(s)$ for the cases of a two section pipe-collar drill-string, and then a two section pipe-collar drill-string connected by a shock-sub. We recall that the axial transfer function is defined as, see (A.12),

$$g_a(s) := -\zeta_a^c \frac{V_b(s)}{W_b(s)}, \tag{20}$$

where ζ_a^c is the nominal impedance at the bottom of the drill-string, which in our case is the impedance of the collar section, i.e. $\zeta_a^c = \frac{A_c E}{c_a}$.

For the case of a pipe-collar–two-section drill-string, we use the two-port configuration from Appendix. This approach is equivalent to first finding the relation between force and velocity at the bottom of the transition between the pipe and the collar sections, $W_p(s)$, $V_p(s)$, and using this as the load impedance for the collar section. I.e., defining (see Fig. 1 for notation.)

$$-\frac{W_p}{V_p} = \frac{\zeta_a^p}{g_a^p(s)}, \qquad g_a^p(s) := \frac{\zeta_a^p}{Z_a^p} \frac{Z_a^p + Z_a^L \tanh \Gamma_a^p}{Z_a^L + Z_a^p \tanh \Gamma_a^p}, \tag{21}$$

we obtain the transfer function of two a section drill-string as

$$g_a(s) = \frac{\zeta_a^c}{Z_a^c} \frac{Z_a^c + \frac{\zeta_a^p}{g_a^p(s)} \tanh \Gamma_a^c}{\frac{\zeta_a^p}{g_a^p(s)} + Z_a^c \tanh \Gamma_a^c}. \tag{22}$$

For more details on this derivation, we refer to (Aarsnes and van de Wouw, 2018).

v_0, ω_0: Axial and angular table velocity

ζ_t^p, ζ_a^p: Pipe impedances
t_t^p, t_a^p: Pipe travel times

V_p: Axial velocity, pipe bottom

X_s: Tool stroke

ζ_t^c, ζ_a^c: Collar impedances
t_t^c, t_a^c: Collar travel times

V_s: Axial velocity, collar top

V_b, Ω_b: Axial and angular bit velocity

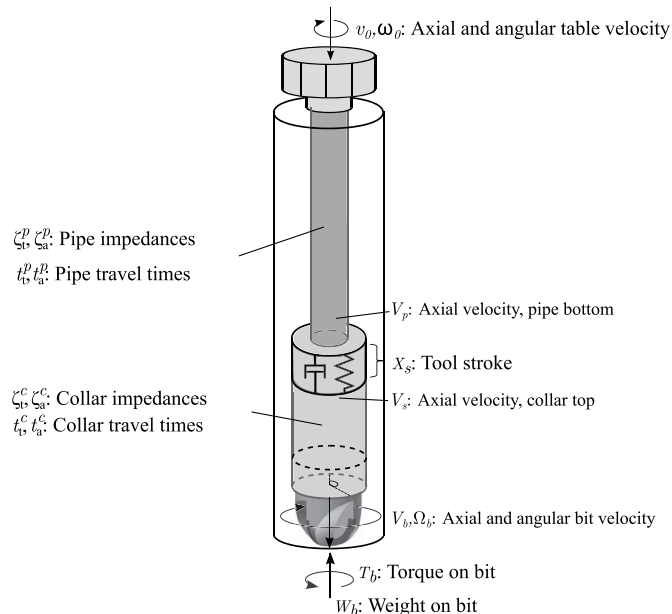T_b: Torque on bit

W_b: Weight on bit

Fig. 1. Schematic of the drill-string.

3.1.1. Two-section drill-string connected by an elastic tool

We consider a shock-sub inserted in the drill-string at the interface between the pipe and collar sections (this location simplifies the analysis to a certain extent; the modeling and analysis framework proposed is however generic), see Fig. 1. The shock-sub is modeled as a spring-damper system with spring and damper constants K_s, D_s. The spring and damper act with the axial force W_s between the collar and pipe sections. Denoting the velocity at the top of the collar section (i.e., at bottom section of the tool) as V_s, the extension/retraction of the tool is given by the difference $V_s - V_p$, and hence we find that the force exerted by the tool is given by

$$-W_p(s) = W_s(s) = (V_s(s) - V_p(s))(K_s/s + D_s), \tag{23}$$

and consequently, combining with (21), we obtain the load seen from the top of the drill collars as $g_a^s(s)$:

$$\frac{W_s}{V_s} = -\frac{\zeta_a^p}{g_a^s}, \qquad g_a^s(s) = \zeta_a^p \frac{(D_s s + K_s) \frac{g_a^p(s)}{\zeta_a^p} + s}{D_s s + K_s}, \tag{24}$$

which allows us to express the axial drill-string transfer function with the elastic tool as

$$g_{a,sub}(s) = \frac{\zeta_a^c}{Z_a^c} \frac{Z_a^c + \frac{\zeta_a^p}{g_a^s(s)} \tanh \Gamma_a^c}{\frac{\zeta_a^p}{g_a^s(s)} + Z_a^c \tanh \Gamma_a^c}. \tag{25}$$

3.2. Shock-sub design: removing the effect of the drill-pipe resonances

In the preceding analysis we observed that unstable modes could be caused by phase variations due to resonances in $g_a(s)$. Removing the effect of these resonances on the axial transfer function simplify the analysis of the drill-string–shock-sub system. We now consider the conditions on the elastic tool such that the resonances caused by the drill pipe above the sub does not influence the below sub dynamics. That is, we determine the conditions under which the effect of the nominal drill-string dynamics, $g_a^s(s)$, has little influence in the $g_{a,sub}(s)$ transfer function in (25). We emphasize that removing the effect of the resonance is *not* a simplification. Instead, we derive conditions on the elastic tool parameters such that the resonances of the drill pipe above the shock sub does not have any influence on the bit-rock BHA dynamics.

The considered system is the same as previously with the parameter values given in Table 2. We note that, since we are able to disconnect the BHA dynamics from the 'above sub' resonances, the result achieved in this section have a wide range of applicability. I.e., changing the parameters of drill string above the BHA will in most cases not have any influence on the stability result.

We denote the mass of the collar section below the elastic tool as

$$M_b = A_c \rho L_c, \tag{26}$$

which facilitates the following lumped (approximative) description of the axial transfer function dynamics:

$$M_b V_b s - W_s + W_b = 0, \tag{27}$$

$$W_s + (V_b - V_s)(K_s/s + D_s) = 0, \tag{28}$$

$$V_s + \frac{1}{\zeta_a^p} g_a^p(s) W_s = 0. \tag{29}$$

(27)–(29) represent three equations with four unknowns which we can solve to obtain the relation

$$\frac{V_b}{W_b} = \frac{-1}{\zeta_a^c} g_{a,sub}(s) \approx -\frac{s + (D_s s + K_s) \frac{g_a^p(s)}{\zeta_a^p}}{M_b s^2 + (D_s s + K_s) M_b \frac{g_a^p(s)}{\zeta_a^p} s + (D_s s + K_s)}. \tag{30}$$

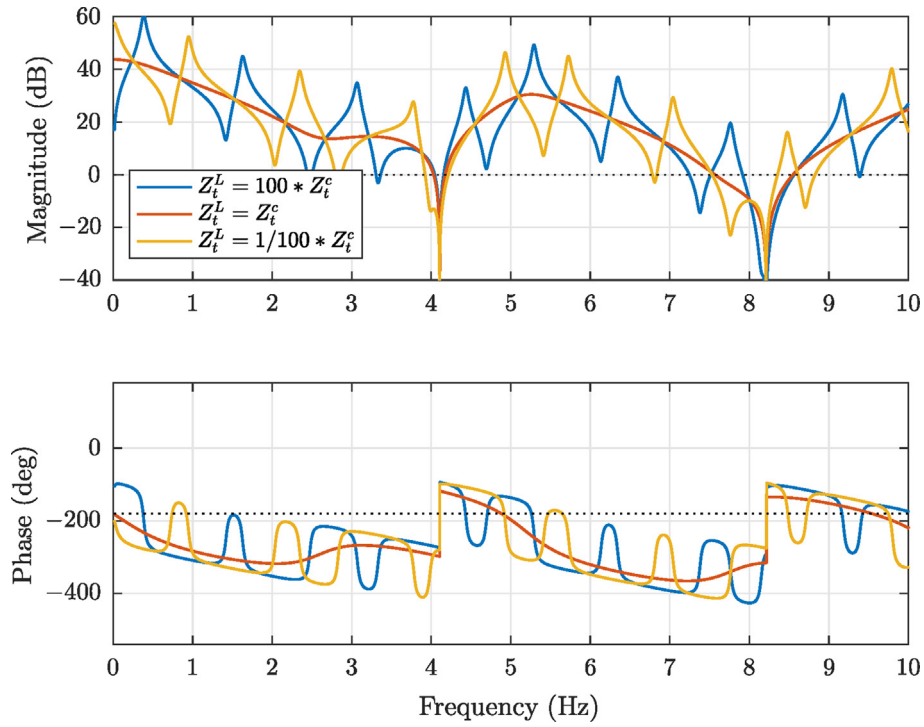To remove the resonance-dominated drill-pipe dynamics above the

Fig. 2. Bode diagram of the torsional term $G_t(s)$ of the characteristic function $G(s)$ for the parameter set given in Table 2. The case of $Z_t^L = 100 Z_t^c$ corresponds to a stiff top-drive, i.e., $\omega_0 \approx$ constant, $Z_t^L = Z_t^c$ reflect impedance matching, while $Z_t^L = (1/100)Z_t^c$ corresponds to a soft top-drive, i.e., $\tau_0 \approx$ constant.

sub, $g_a^p(s)$, from the bit-rock interaction dynamics we require

$$\left| \frac{(D_s s + K_s)}{s} \frac{g_a^p(s)}{\zeta_a^p} \right| \ll 1 \tag{31}$$

Namely, if this is achieved we can approximate (30) with

$$g_{a,sub}(s) \approx \frac{s \zeta_a^c}{M_b s^2 + D_s s + K_s}. \tag{32}$$

Typical feasible values for a shock sub stiffness is $K_s \leq 10^4$ N/m (see, e.g. (Weatherford, 2010)), while D_s is assumed small in comparison. The effect of inserting such a sub and the validity of the approximation in (32) is shown in Fig. 4. This figure shows the transfer function of the
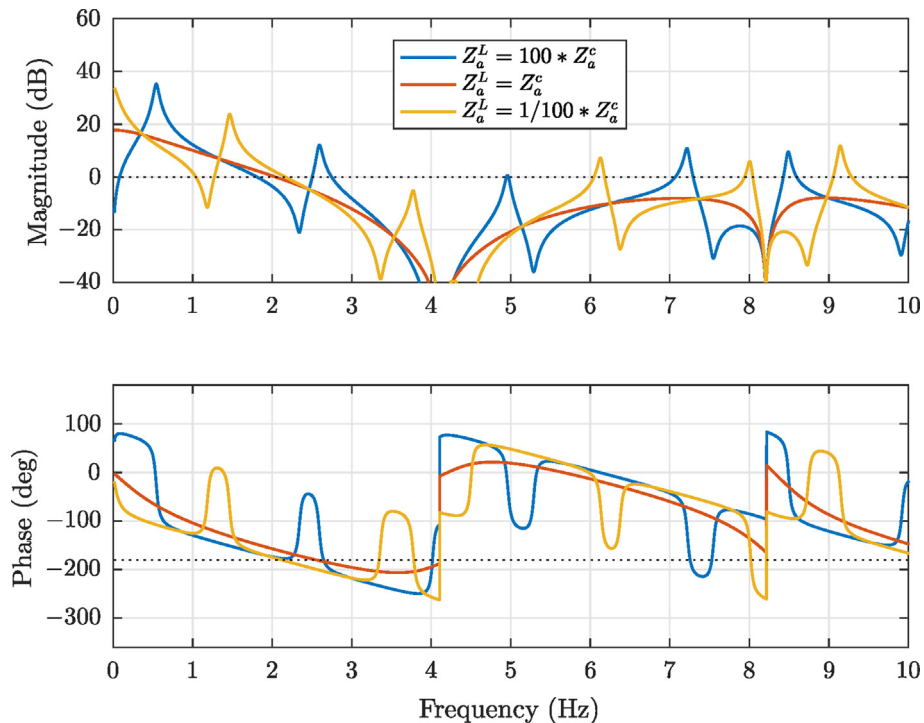

Fig. 3. Bode diagram of the axial term $G_a(s)$ of the characteristic function $G(s)$ for the parameter set given in Table 2. The case of $Z_a^L = 100 Z_a^c$ corresponds to a stiff top-drive, i.e., $v_0 \approx$ constant, while $Z_a^L = Z_a^c$ reflect impedance matching and $Z_a^L = (1/100)Z_a^c$ corresponds to a soft top-drive, i.e., $w_0 \approx$ constant.
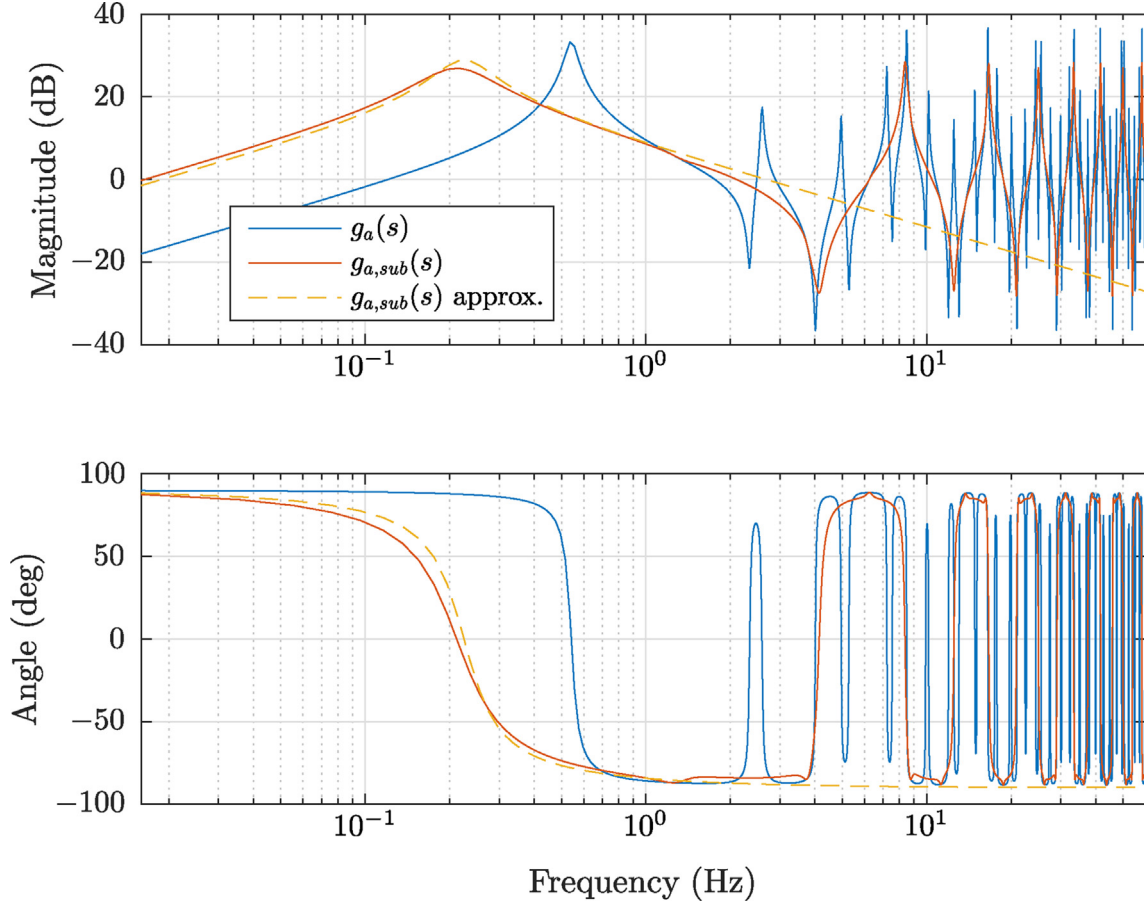
Fig. 4. Bode plot showing the shock-sub effectively removing the resonant axial drill-string dynamics from the transfer function. The approximation used to simplify the design is also shown, and is observed to be valid in the critical range around the first cross-over frequency.

drill string without the sub, '$g_a(s)$', with the sub, '$g_{a,sub}(s)$' and the approximation used to design the sub, '$g_{a,sub}(s)$ approx'. It can be observed that the lumped approximation is successful in representing the first resonance mode of '$g_{a,sub}(s)$' occurring at $\sqrt{\frac{K_s}{M_b}}\frac{1}{2\pi} \approx 0.23$ [Hz], but the fit becomes poor for high frequencies when the fast distributed compression dynamics of the drill collars becomes important. In particular, we note the internal high-frequency resonant modes of the drill collars. However, the resonances of the pipe section seen in '$g_a(s)$', are effectively removed, which was the goal pursued. This simplifies the stability analysis, performed in the next section, and consequently allows us to derive conditions which ensure stability.

3.3. Axial stability analysis with the elastic tool

From (32), assuming that the effect of the axial resonances in the pipe section above the shock-sub have been removed, we can employ the following approximation for the axial loop characteristic equation

$$G_a(s) = g_{a,sub}(s)\frac{K_a}{s}\left(1 - e^{-t_N s}\right), \tag{33}$$

$$\approx \frac{a\zeta\varepsilon N}{M_b s^2 + D_s s + K_s}\left(1 - e^{-t_N s}\right). \tag{34}$$

Before the occurrence of the resonance, the phase contribution of the drill string factor $g_{a,sub}$ is positive, and hence no instability can occur. After the occurrence of the resonance, i.e. $\omega > \sqrt{\frac{K_s}{M_b}}$, the factors in (33) have the following phase contributions

$$\arg\frac{a\zeta\varepsilon N}{M_b s^2 + D_s s + K_s} = -180\mathrm{deg}, \tag{35}$$

$$\arg\left(1 - e^{-t_N s}\right) \in [-90,90]\mathrm{deg}. \tag{36}$$

Consequently, we find that condition **A1**, in (12), is satisfied when the phase contribution of the delay crosses zero, i.e. when $e^{-t_N s} = 1$. To avoid instabilities, the low-pass factor introduced by the down-hole tool must roll of sufficiently before this point. In other words, the transfer function in (34) looses magnitude for higher frequencies above the resonance, and we require that the magnitude is less than $-6dB$ when the phase contribution of the delay crosses zero. This is shown in Fig. 5, where the green dotted line indicates the frequency where the phase contribution of the delay crosses zero, at which point $|1 - e^{-t_N s}| = 6$ dB.

Noting that this occurs at $\omega = \pi/t_N$ radians per second (i.e., equivalent with the frequency $\frac{1}{2t_N}$ Hertz) where we have $|1 - e^{-s t_N n}|_{\omega=\pi/t_N} = 2$, we obtain the following requirement

$$|G_a(\omega = \pi/t_N)| < 1, \tag{37}$$

$$\Leftrightarrow \left|\frac{2a\zeta\varepsilon N}{M_b\left(\frac{\pi}{t_N}\right)^2 + D_s\frac{\pi}{t_N} + K_s}\right| < 1. \tag{38}$$

Noting that the second-order term in the denominator in (38) will dominate at higher frequency, we obtain the following slightly conservative simplification of (38):

$$M_b > \frac{2a\zeta\varepsilon N t_N^2}{\pi^2}. \tag{39}$$

Recalling that the delay is related to the rotational velocity as $t_N = \frac{2\pi}{N\omega_0}$, we can write (39) as:

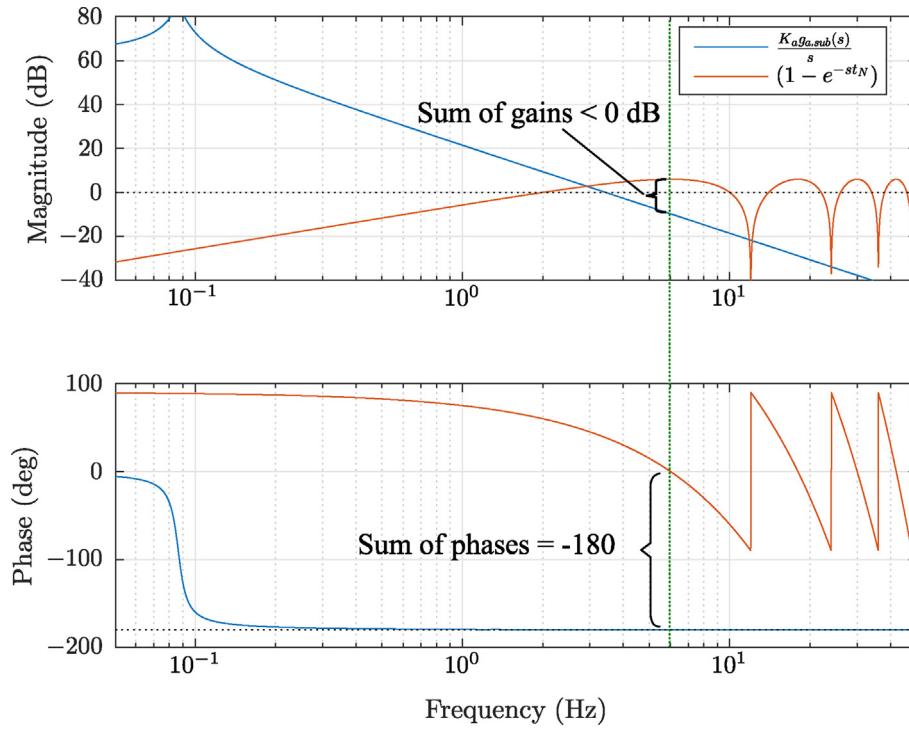$$M_b\omega_0^2 > 8\frac{a\zeta\varepsilon}{N}. \tag{40}$$

Fig. 5. Conceptual Bode diagram of the simplified open-loop transfer function illustrating the principle of the analysis. Note that the product of gains is summed to find the total gain when denoted in dB (which is a logarithmic scale).

This inequality imposes a condition on the minimum size of the mass below the sub M_b, given a bit geometry, bit-rock parameters: a, ζ, ε, N and a desired RPM, ω_0. The appropriate weight can be obtained in design by placing the sub at the correct position in the drill-string.

For the parameters in Table 2, (40) equates to

$$M_b > 50.15 * 10^3 \text{ kg.} \tag{41}$$

I.e., a collar section of 300 m.

To summarize the preceding approach:

1. The tool parameters K_s, D_s only influence the shape of the first resonance.
2. Designing K_s, D_s such that (31) is satisfied, allows for the approximation (32).
3. When approximation (32) is valid, stability is determined by (40). That is, stability is determined by tool location, and not on the tool stiffness and damping parameters, K_s, D_s.

Remark 1. The same relation (40) was found to define the critical rotation speed in (Depouhon and Detournay, 2014), at which "the system switches from the fast instability regime to the slow one". This analysis was done on a simplified single lumped mass approximation of the drill-string. When a lower section of the drill-string is isolated from the rest through the use of an axial high-elasticity sub, as proposed above, such a lumped-parameter model approximation might be amenable. When the lumped section becomes too long, however, the approximation is no longer valid as distributed effects in the drill collars start to become important also for the BHA part below the down-hole tool. This situation is considered next.

3.4. On the influence of drill collar dynamics

The main limiting factor of accomplishing the approach described in the preceding section is the stringent requirement on the mass below the tool, M_b, to achieve sufficient high-frequency roll-off for stability. To satisfy this requirement, the section of pipe/collars below the tool might have to be made rather long, i.e., several hundred meters long. In this case, the distributed nature of this section also might become of importance.

Consider again the drill-string transfer function shown in Fig. 4. It can be observed that the lumped approximation is successful in representing the first resonant mode, but the fit becomes poor for high frequencies when the fast distributed compression dynamics of the drill collars becomes important. In particular we note the internal high-frequency resonant modes of the drill collars. We know that these high-frequency dynamics are due to the distributed collar dynamics because all high-frequency dynamics in the drill string have been disconnected from the collar section by the elastic tool. These high-frequency resonant modes can cause instabilities. However, in the case of such an instability, the resulting limit cycle will occur at a higher frequency, corresponding to the higher frequency at which the unstable mode is located, and the effect of the instability on slow time-scale behavior (such as ROP) could be qualitatively different. The impact of such high-frequency vibrations is still an open research topic.

3.5. Resonance-delay matching

As discussed above, the high-frequency dynamics of the drill collar below the elastic tool can cause instabilities. A novel approach to avoid also these high-frequency unstable modes is to tune the set-point of the rotation rate ω_0 to the length of drill collar section below the shock sub. Similar analysis techniques for delay systems have been investigated in the context of electroaccoustics (Zhang and Stepan, 2016). Specifically, we note from **Condition A1** in (12) that axial instability only can occur when the phase contribution of $g_{a,sub}(s)$ and the delay term are both negative. In particular, the critical part of the frequency range is when $g_{a,sub}(s)$ both has a large magnitude and negative phase contribution, which is in frequency range after a resonance has occurred, specifically for frequencies such that:

$$n_1 \frac{c_a}{2L_c} < f < n_1 \frac{c_a}{2L_c} + \frac{1}{8\pi} \quad \text{[Hz]}, \quad n_1 = 1,2, ..., \tag{42}$$
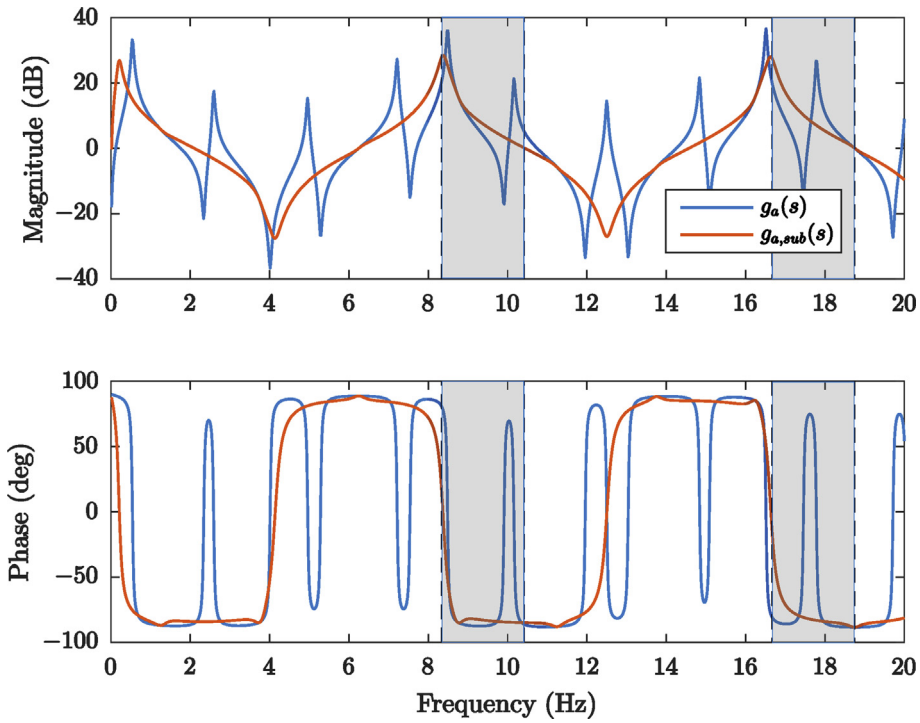
Fig. 6. The axial drill-string transfer function $g_a(s)$ with and without the shock-sub, and with the critical frequency ranges indicated in grey.

where L_c is the length of the drill collar section below the shock sub, and c_a is the speed of the axial compression waves. This frequency range is indicated in Fig. 6. The phase contribution of the delay term is negative when:

$$N\frac{\omega_0}{2\pi}(n_2 - 1/2) < f < N\frac{\omega_0}{2\pi}n_2 \text{ [Hz]}, \quad n_2 = 1,2.... \tag{43}$$

That is, to avoid instability being caused by the drill collar dynamics we want to avoid (42) and (43) being satisfied at the same time for the first couple modes n_1. At higher frequencies (corresponding to higher mode number n_1) the axial term $G_a(s)$ in (33) rolls off due to the integral factor, reducing the gain. Hence, we obtain the heuristic that instability can be avoided by setting

$$\omega_0 = \frac{1}{n}\frac{\pi c_a}{NL_c} - \varepsilon_\omega, \quad n = 1,2,... \tag{44}$$

where $\varepsilon_\omega > 0$ is small.

As an example of this approach, we consider a case with a down-hole tool with the parameters in Table 3, and the system parameters in Table 2. A rotation rate of 61.5 RPM is chosen, corresponding to (44) with $n = 2$ and $\varepsilon_\omega = 1$ RPM.

The resulting Bode diagram for the axial term $G_a(s)$, with and without the tool, is given in Fig. 7 and corresponding Nyquist chart in Fig. 8. Using the Nyquist criterion, see Theorem 1 in (Aarsnes and van de Wouw, 2018), we observe that the Nyquist contour $\Gamma_{G_a(s)}$, without the down-hole tool, encircles the -1 point several times, indicating unstable poles. The Nyquist contour of the axial transfer function with the down-hole tool $\Gamma_{G_a(s)}$ does not encircle -1 indicating stability of the axial dynamics. Hence, by using the design of the shock sub and the resonance-delay matching it is ensured that neither the low-frequency drill-pipe resonances nor the high-frequency collar dynamics can lead

Table 3
Elastic tool parameters.

$M_b=$	50×10^3	kg
$D_s=$	30×10^3	Ns/m
$K_s=$	100×10^3	N/m

to instability.

We note that, since the shock-sub only affects the axial dynamics, the torsional term in the characteristic equation, $G_t(s)$, is not changed by the inclusion of the shock-sub. Consequently, impact of the shock sub on the potential occurrence of stick slip vibrations can not be assessed from only the local stability analysis as performed in this section.

4. Time-domain simulation study

In this section, we compare the results from the frequency-domain considerations to those of a simulation study of a non-linear simulation model, hence analyzing the global axial dynamics of the system. For the simulation model, we use an implementation which is an extension of the one presented in (Aarsnes and van de Wouw, 2019) by including the shock subs model. This implementation is described in Appendix C.

4.1. Simulation results

The drill-string model, with the same parameter set that was considered for the local frequency-domain analysis (i.e., with the parameters of Table 2), is now considered for non-local, time-domain analysis.

Two simulations are performed, one with just the two-section drill-string, and one where the pipe and collar sections are connected with the proposed elastic tool with the parameters of Table 3. That is, the simulation is performed with the same model considered in the frequency-domain analysis, including the resonance-delay matching RPM of 61.5. The resulting axial and angular bit velocities are shown in Fig. 9. This simulation confirms the finding of the local frequency-domain analysis, in that for the considered case the elastic tool removes the axial instability, see top figure in Fig. 9. The axial and torsional dynamics are coupled through the non-linearity in the bit–rock interaction (A.9)–(A.11). Hence, in this case, by achieving stable axial dynamics the non-linearity is not activated resulting in stable torsional dynamics in the simulation with the shock sub, see the bottom figure in Fig. 9. It should be noted, however, that the axial–torsional coupling in this model is quite complex and it is difficult to draw general
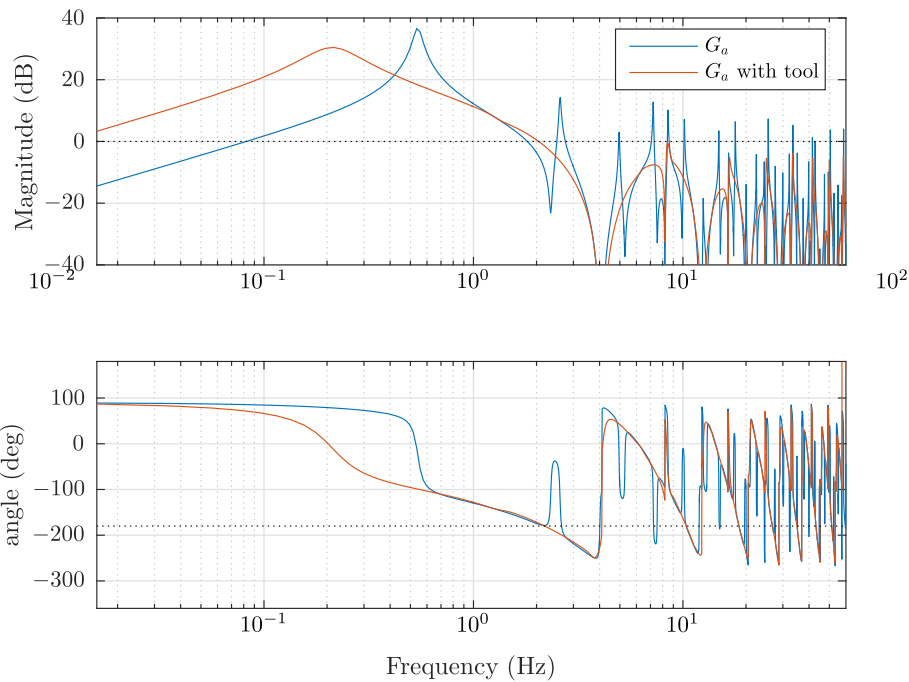
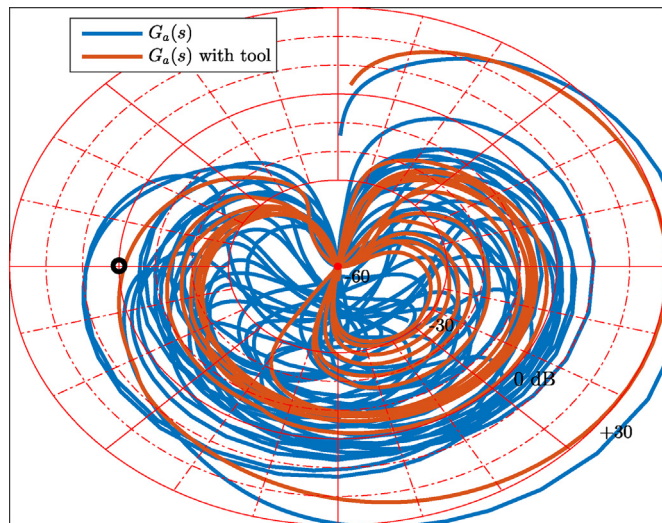**Fig. 7.** The axial transfer function $G_a(s)$ with and without the sub.

Fig. 8. Logarithmic Nyquist chart of the axial term $G_a(s)$ with and without the elastic tool. For this case, the elastic tool stabilizes the axial dynamics.

conclusions. That is, although improved torsional behavior (i.e., angular bit velocity converges to its equilibrium) is achieved in the simulation considered in this section, we cannot conclude that this would be the result in the general case. This issue, on the complex linear and non-linear coupling between the axial and torsional dynamics, is discussed at length in (Aarsnes and van de Wouw, 2019) for the case of a drill-string system without a shock-sub.

Appendix A. Model description

This section derives the mathematical description of the pipe–collar drilling system depicted in Fig. 1 (with and without the indicated tool). First, we introduce a distributed model of axial–torsional drill-string dynamics. Next, the axial–torsional dynamics are coupled through a non-linear bit–rock interaction law described as a transport equation. Finally, the frequency-domain description of the linearized model is given.

5. Conclusions

In this paper, we have performed a frequency-domain analysis of the effect of a downhole axial elastic tool (shock sub) on the distributed dynamics of the drill string. We have shown that the axial instability, caused by the regenerative effect of the bit–rock interaction, can be manipulated by the placement of an elastic tool. In particular, it has been shown that the slow unstable mode can be stabilized by having a sufficiently large mass below the tool, while to avoid high-frequency unstable modes the rotational velocity of the top-drive (RPM) has to be tuned to the resonances of the section below the tool (collar section). The ability of the elastic tool to stabilize the axial dynamics have been confirmed through a time-domain simulation study using a non-local model incorporating the non-linearities of the bit–rock interaction.

The analysis does not include the effect of interaction between the drill-string and the borehole. Still, we argue that this approximation is a reasonable first step in investigating the effect of shock subs on self-excited vibrations. We project that the results presented in this paper can be constructively build upon in future work taking additional effects into account.
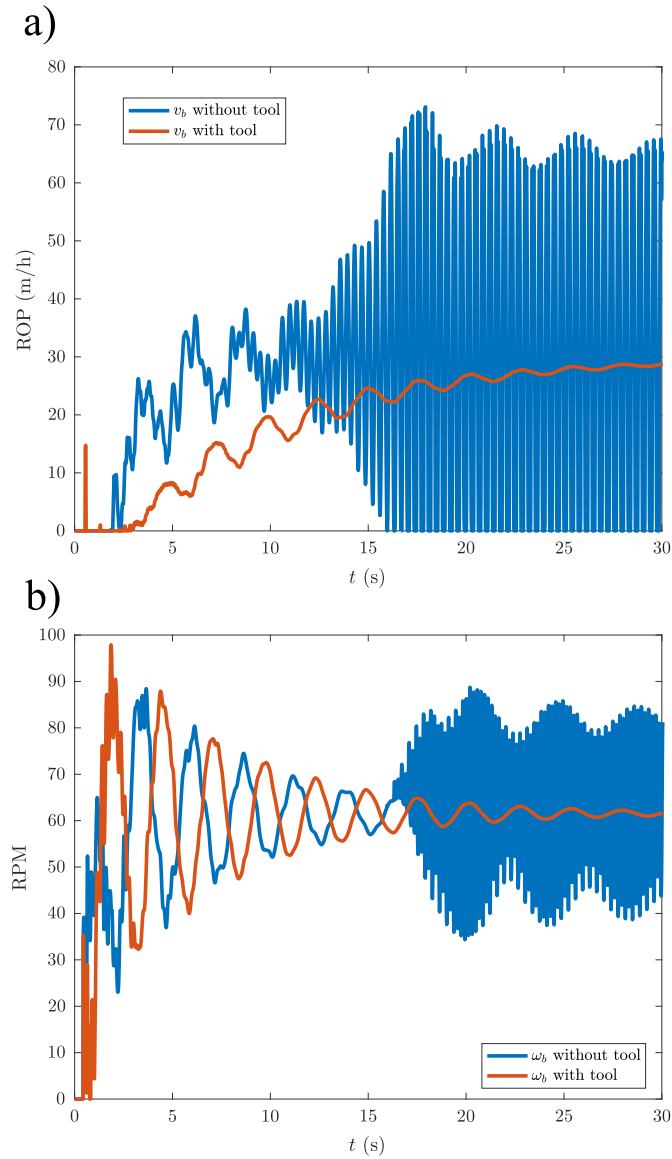
a)

b)

Fig. 9. Time series comparison of **a)** ROP and **b)** RPM, with and without the elastic tool (shock sub).

Appendix A.1. Distributed drill-string model

We employ the distributed drill-string model as derived in (Aarsnes and Aamo, 2016; Aarsnes and van de Wouw, 2018; Germay et al., 2009b). In the following exposition the model equations are restated without explanations, and we refer to (Aarsnes and van de Wouw, 2018), where the same notation is used, for a more detailed derivation.

Let $v(t, x)$, $w(t, x)$ denote axial velocity and force, and $\omega(t, x)$, $\tau(t, x)$ the angular velocity and torque, where $(t, x) \in [0, \infty) \times [0, L]$ with t the times, x the spacial coordinate and L the length of the drill-string. Then the axial dynamics are described by

$$\frac{\partial w(t, x)}{\partial t} + A_i E \frac{\partial v(t, x)}{\partial x} = 0 \tag{A.1}$$

$$A_i \rho \frac{\partial v(t, x)}{\partial t} + \frac{\partial w(t, x)}{\partial x} = -k_a \rho A_i v(t, x), \tag{A.2}$$

and the torsional dynamics by

$$\frac{\partial \tau(t, x)}{\partial t} + J_i G \frac{\partial \omega(t, x)}{\partial x} = 0 \tag{A.3}$$

$$J_i \rho \frac{\partial \omega(t, x)}{\partial t} + \frac{\partial \tau(t, x)}{\partial x} = -k_t \rho J_i \omega(t, x). \tag{A.4}$$

Here, A_i is the cross sectional area of the drill-string, E is the Young's modulus, where $i \in \{p, c\}$ for the pipe and collar section, respectively, ρ denotes the pipe mass density, k_a, k_t are viscous damping coefficients, J_i the polar moment for inertia and G the shear modulus.

The drill-string is coupled with the bit-rock interaction at the boundary through the right-side (downhole) boundary condition

$$w(t, x = L) = w_b, \qquad \tau(t, x = L) = \tau_b, \tag{A.5}$$

while at the left boundary (topside) the torsional boundary condition is given by a specified top drive velocity

$$\omega(t, x = 0) = \omega_0. \tag{A.6}$$

At the axial topside boundary, a constant axial velocity is imposed:

$$v(t, x = 0) = v_0. \tag{A.7}$$

The bit–rock interaction determining w_b and τ_b in (A.5) are described next.

Appendix A.1.1. Bit-rock interaction law

We use the bit-rock interaction law of (Detournay and Defourny, 1992), but in the equivalent reformulation as a transport equation description due to (Gupta and Wahi, 2016; Wahi and Chatterjee, 2008). We refer to (Aarsnes and van de Wouw, 2019) for a description including the distributed drill string.
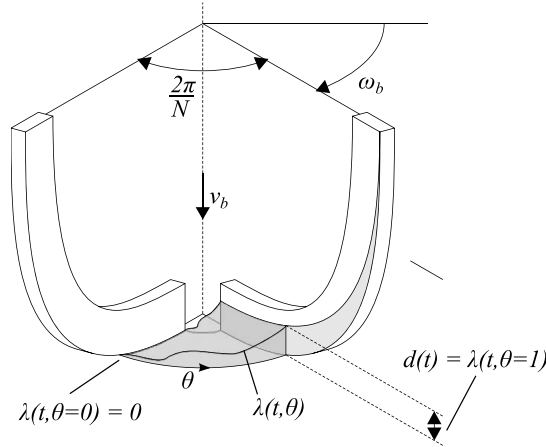

Fig. A.10. Bit rock interaction.

The evolution of the uncut cut rock between two blades, see Figure A.10, relative to bit position, is given by $\lambda(t, \theta)$, with $\theta \in [0,1]$ denoting the normalized angle between a cutter at the bit to a point at the bit, see Fig A.10. The evolution of λ can be described by the transport equation

$$\frac{\partial \lambda(t, \theta)}{\partial t} + \omega_b(t) \frac{N}{2\pi} \frac{\partial \lambda(t, \theta)}{\partial \theta} = v_b(t), \tag{A.8}$$

where $v_b(t)$, $\omega_b(t)$ are the axial and angular bit velocities, respectively, i.e., $v_b(t) = v(t, x = L)$, $\omega_b(t) = \omega(t, x = L)$. Consequently, the depth of cut is given as $d(t) = \lambda(t, 1)$.

Following (Detournay and Defourny, 1992), the axial force on bit is given as

$$w_b(t) = a \zeta \varepsilon N d(t), + w_f g(v_b(t)), \tag{A.9}$$

$$g(v_b) = \frac{1 - \text{Sign}(v_b)}{2} = \begin{cases} 0, & v_b < 0 \\ [0,1], & v_b = 0, \\ 1, & v_b > 0 \end{cases} \tag{A.10}$$

where the $a\zeta\varepsilon Nd$ term is due to the cutting force with a the bit radius, ζ is a cutter sharpness coefficient and ε is the rock intrinsic specific energy. The second term, $w_f g(v_b)$, denotes the wear flat force component where w_f is the normal force that must be overcome before axial cutting is initiated, while the non-linear function $g(v_b)$ (colloquially referred to as the $g(\cdot)$ non-linearity) is a set-valued map described in (Besselink et al., 2011). Similarly for the torque on bit, we have

$$\tau_b = a^2 \varepsilon N d + \tau_f g(v_b). \tag{A.11}$$

Appendix A.2. Frequency-domain model description

Here we restate the equations of the dynamics in the frequency domain. A comprehensive description is given by (Aarsnes and van de Wouw, 2018), which again builds on (Aarsnes and Aamo, 2016; Dwars, 2015). The Laplace transformed variables are indicated by capital letters, with the independent parameter $s \in \mathbb{C}$ denoting the Laplace variable.

For the axial dynamics, $g_a(s)$ relates weight on bit W_b to axial bit velocity V_b as follows:

$$\frac{V_b}{W_b}(s) = -\frac{1}{\zeta_a^i} g_a(s), \qquad g_a(s) := \frac{\zeta_a^i}{Z_a^i} \frac{Z_a^i + Z_a^L \tanh \Gamma_a^i}{Z_a^L + Z_a^i \tanh \Gamma_a^i}, \tag{A.12}$$

while for the torsional dynamics $g_t(s)$ relates torque on bit T_b to angular bit velocity Ω_b as follows:

$$\frac{\Omega_b}{T_b}(s) = -\frac{1}{\zeta_t}g_t(s), \quad g_t(s): =\frac{\zeta_t^i \, Z_t^i + Z_t^L \tanh \Gamma_t^i}{Z_t^i \, Z_t^L + Z_t^i \tanh \Gamma_t^i}.$$

(A.13)

Here the axial and torsional characteristic line impedances Z_a^i, $i \in \{p, c\}$, and Z_t^i, $i \in \{p, c\}$, and propagation operators, Γ_a^i, $i \in \{p, c\}$, and Γ_t^i, $i \in \{p, c\}$, are given as

$$Z_a^i(s) = \zeta_a^i\left(1 + \frac{k_a}{\rho s}\right)^{1/2}, \ \Gamma_a^i(s) = st_a^i\left(1 + \frac{k_a}{\rho s}\right)^{1/2},$$

(A.14)

with $\zeta_a^i := \frac{A_i E}{c_a}$, $t_a^i := \frac{L_i}{c_a}$, and

$$Z_t^i(s) = \zeta_t^i\left(1 + \frac{k_t}{\rho s}\right)^{1/2}, \ \Gamma_t^i(s) = st_t^i\left(1 + \frac{k_t}{\rho s}\right)^{1/2},$$

(A.15)

with $\zeta_t^i := \frac{J_i G}{c_t}$, $t_t^i := \frac{L_i}{c_t}$, and where $c_a = \sqrt{E/\rho}$, $c_t = \sqrt{G/\rho}$ denoting the axial and torsional wave velocities, respectively. The transfer functions $Z_t^L(s)$, $Z_a^L(s)$ denotes the torsional and axial load impedances, respectively, which are transfer functions given by the Laplace transform of the dynamics at the topside boundary. Specifically, in the general case these are given as

$$Z_t^L(s): =\frac{T_0}{\Omega_0}(s), \qquad Z_a^L(s): =\frac{W_0}{V_0}(s),$$

(A.16)

while for the BCs (A.7), (A.6), these are $Z_t^L = Z_a^L = \infty$.

The linearized bit-rock interaction law writes (in the Laplace domain)

$$W_b(s) = a\zeta \varepsilon D(s), \quad T_b(s) = \frac{1}{2}a^2\varepsilon D(s),$$

(A.17)

and

$$D(s) = \frac{N}{s}\left[V_b(s)\left(1 - e^{-t_N s}\right) - \frac{\bar{v}}{\omega_0}\Omega_b(s)\left(1 - e^{-t_N s}\right)\right],$$

(A.18)

where $D(s)$ is the Laplace transform of the combined depth of cut $Nd(t) = N\lambda(t, 1)$ in (A.1), and $t_N = \frac{2\pi}{N\omega_0}$.

Appendix B. Combining drill-string subsections

Assume we have a two-port series, and load impedance, specification of a drill-string on the form:

$$\begin{bmatrix} W_2 \\ V_2 \end{bmatrix} = \mathbf{M_{21}}(s)\begin{bmatrix} W_1 \\ V_1 \end{bmatrix},$$

(B.1)

$$\begin{bmatrix} W_1 \\ V_1 \end{bmatrix} = \mathbf{M_{10}}(s)\begin{bmatrix} W_0 \\ V_0 \end{bmatrix},$$

(B.2)

$$W_0 = Z_L(s)V_0,$$

(B.3)

where $\mathbf{M_{21}}(s)$, $\mathbf{M_{10}}(s): \mathbb{C} \to \mathbb{C}^{2\times 2}$ are transfer matrices. Now write

$$\begin{bmatrix} W_2 \\ V_2 \end{bmatrix} = \mathbf{M_{21}}\mathbf{M_{10}}\begin{bmatrix} W_0 \\ V_0 \end{bmatrix} =: \begin{bmatrix} A_1(s) & A_2(s) \\ B_1(s) & B_2(s) \end{bmatrix}\begin{bmatrix} W_0 \\ V_0 \end{bmatrix}.$$

(B.4)

The transfer function relation between the velocity and force at position 2 can now be found by observing

$$W_2 = (A_1(s)Z_L(s) + A_2(s))V_0 =: \bar{A}(s)V_0$$

(B.5)

$$V_2 = (B_1(s)Z_L(s) + B_2(s))V_0 =: \bar{B}(s)V_0$$

(B.6)

and hence

$$\frac{W_2}{V_2}(s) = \frac{\bar{A}(s)}{\bar{B}(s)}.$$

(B.7)

Appendix C. Simulation model

Appendix C.1. Derivation of Riemann invariants

The following derivation is shown for the torsional dynamics only for the sake of brevity. The derivation for the axial dynamics is equivalent. Define the Riemann invariants

$$\alpha = \omega + \frac{c_t}{JG}\tau, \quad \beta = \omega - \frac{c_t}{JG}\tau,$$

(C.1)

where $c_t = \sqrt{\frac{\rho}{J}}$ is the velocity of the torsional wave. Using (C.1) in (A.3),(A.4), it can be shown that the variables α, β satisfies the diagonalized PDE system:

$$\frac{\partial \alpha}{\partial t} + c_t \frac{\partial \alpha}{\partial x} = -k_t(\alpha + \beta) \tag{C.2}$$

$$\frac{\partial \beta}{\partial t} - c_t \frac{\partial \beta}{\partial x} = -k_t(\alpha + \beta). \tag{C.3}$$

Appendix C.2. Discontinuities of a multi-section drill-string

At the discontinuity of the pipe-collar intersection we have to enforce the following continuity conditions:

$$\omega^+ = \omega^-, \qquad \tau^+ = \tau^-, \tag{C.4}$$

which entail, in terms of the Riemann invariants,

$$\beta^+ = \frac{1}{1 + \bar{Z}}(\alpha^+(1 - \bar{Z}) + 2\bar{Z}\beta^-) \tag{C.5}$$

$$\alpha^- = \frac{1}{1 + \bar{Z}}(2\alpha^+ - (1 - \bar{Z})\beta^-) \tag{C.6}$$

where we have denoted the relative magnitude of the impedance as

$$\bar{Z} = \left[\frac{c_t}{JG}\right]^- / \left[\frac{c_t}{JG}\right]^+. \tag{C.7}$$

We note that for the case of the same material being used at both sides of the discontinuity, the only change is in the polar moment of inertia J_i $i \in \{p, c\}$. That is, for a pipe-collar sections of e.g. steel, we have,

$$\bar{Z} = \frac{J_c}{J_p}. \tag{C.8}$$

Note the meaning of (C.5)–(C.6) as reflections of incoming waves from both sides, as they are split into an upward and a downward traveling wave. The model equations are then integrated numerically with an upwind scheme.

Appendix C.3. Numerical implementation

In the numerical implementation of the model, the wave equations (A.1), (A.2) and (A.3), (A.4), are transformed into their Riemann invariants (LeVeque, 2002) and all the five resulting transport equations of the system, including (A.8), are then solved with a first-order upwind scheme (Patankar, 1980). A first-order scheme is used to avoid spurious oscillations, as it was found that higher-order schemes performed poorly due to the temporal discontinuities introduced by the differential inclusions in the bit-rock interaction.

In all simulations, a spatial grid of 400 cells is used for the combined pipe-collar drill-string model and the time-step was chosen so as to enforce a Couran-Friedrichs-Lewy (CFL) number of at least 0.9. The cell number for (A.1) was then chosen such that the CFL condition is enforced (Courant et al., 1967).

References

Aarsnes, U.J.F., Aamo, O.M., 2016. Linear stability analysis of self-excited vibrations in drilling using an infinite dimensional model. J. Sound Vib. 360, 239–259. https://doi.org/10.1016/j.jsv.2015.09.017.

Aarsnes, U.J.F., Shor, R.J., 2018a. Torsional vibrations with bit off bottom: modeling, characterization and field data validation. J. Pet. Sci. Eng. 163, 712–721. https://doi.org/10.1016/j.petrol.2017.11.024.

Aarsnes, U.J.F., Shor, R.J., 2018b. Stick-slip and torsional friction factors in inclined wellbores. In: MATEC Web of Conferences, vol. 148https://doi.org/10.1051/matecconf/201814816002.

Aarsnes, U.J.F., van de Wouw, N., 2018. Dynamics of a distributed drill string system: characteristic parameters and stability maps. J. Sound Vib. 417, 376–412. https://doi.org/10.1016/j.jsv.2017.12.002.

Aarsnes, U.J.F., van de Wouw, N., 2019. Axial and torsional self-excited vibrations of a distributed drill-string. J. Sound Vib. 444 (March), 127–151. https://doi.org/10.1016/j.jsv.2018.12.028.

Aarsnes, U.J.F., Auriol, J., Di Meglio, F., Shor, R.J., 2019. Estimating friction factors while drilling. J. Pet. Sci. Eng. 179, 80–91. https://doi.org/10.1016/j.petrol.2019.04.014.

Bailey, J.R., Remmert, S.M., 2010. Managing drilling vibrations through BHA design optimization. SPE Drill. Complet. 25 (04), 458–471. https://doi.org/10.2118/139426-PA.

Besselink, B., van de Wouw, N., Nijmeijer, H., 2011. A semi-analytical study of stick-slip oscillations in drilling systems. J. Comput. Nonlinear Dyn. 6 (2), 021006. https://doi.org/10.1115/1.4002386.

Besselink, B., Vromen, T., Kremers, N., van de Wouw, N., 2016. Analysis and control of stick-slip oscillations in drilling systems. IEEE Trans. Control Syst. Technol. 24 (1), 226–239. https://doi.org/10.1109/TCST.2015.2502898.

Courant, R., Friedrichs, K., Lewy, H., 1967. On the partial difference equation of mathematical physics. IBM J. Res. Dev. 11 (215–234), 32–74. https://doi.org/10.1147/rd.112.0215. arXiv:AD0832715.

Depouhon, A., Detournay, E., 2014. Instability regimes and self-excited vibrations in deep drilling systems. J. Sound Vib. 333 (7), 2019–2039. https://doi.org/10.1016/j.jsv.2013.10.005.

Detournay, E., Defourny, P., 1992. A phenomenological model for the drilling action of drag bits. Int. J. Rock Mech. Min. Sci. Geomech. Abstr. 29 (1), 13–23. https://doi.org/10.1016/0148-9062(92)91041-3.

Dunayevsky, V., Abbassian, F., 1998. Application of stability approach to bit dynamics. SPE Drill. Complet. 13 (02), 99–107. https://doi.org/10.2118/30478-PA.

Dwars, S., 2015. Recent advances in soft torque rotary systems. In: SPE/IADC Drilling Conference and Exhibition. Society of Petroleum Engineers, London, United Kingdom, pp. 29–44. https://doi.org/10.2118/173037-MS. No. March.

Germay, C., van de Wouw, N., Nijmeijer, H., Sepulchre, R., 2009a. Nonlinear drillstring dynamics analysis. SIAM J. Appl. Dyn. Syst. 8 (2), 527–553. https://doi.org/10.1137/060675848.

Germay, C., Denoël, V., Detournay, E., 2009b. Multiple mode analysis of the self-excited vibrations of rotary drilling systems. J. Sound Vib. 325 (1–2), 362–381. https://doi.org/10.1016/j.jsv.2009.03.017.

Ghasemloonia, A., Geoff Rideout, D., Butt, S.D., 2015. A review of drillstring vibration modeling and suppression methods. J. Pet. Sci. Eng. 131, 150–164. https://doi.org/10.1016/j.petrol.2015.04.030.

Gupta, S.K., Wahi, P., 2016. Global axial–torsional dynamics during rotary drilling. J. Sound Vib. 375, 332–352. https://doi.org/10.1016/j.jsv.2016.04.021.

Gupta, S.K., Wahi, P., 2018. Tuned dynamics stabilizes an idealized regenerative axial-torsional model of rotary drilling. J. Sound Vib. 412, 457–473. https://doi.org/10.1016/j.jsv.2017.08.044.

Insperger, T., Stépán, G., Turi, J., 2006. State-dependent delay in regenerative turning processes. Nonlinear Dynam. 47 (1–3), 275–283. https://doi.org/10.1007/s11071-006-9068-2.

Jardine, S., Malone, D., Sheppard, M., 1994. Putting a damper on drilling's bad vibrations. Oilfield Rev. 1 (January), 15–20.

Kalmár-Nagy, T., Stépán, G., Moon, F.C., 2001. Subcritical hopf bifurcation in the delay equation model for machine tool vibrations. Nonlinear Dynam. 26 (2), 121–142. https://doi.org/10.1023/A:1012990608060.

Kyllingstad, Å., Nessjøen, P.J., March, 2009. A new stick-slip prevention system. In:

Proceedings of SPE/IADC Drilling Conference and Exhibition, pp. 17–19. https://doi.org/10.2118/119660-MS.

LeVeque, R.J., 2002. Finite Volume Methods for Hyperbolic Problems. Cambridge university press.

Nishimatsu, Y., 1972. The mechanics of rock cutting. Int. J. Rock Mech. Min. Sci. 9 (February 1971), 261–270.

Patankar, S., 1980. Numerical Heat Transfer and Fluid Flow. CRC press, New York, NY.

Richard, T., Germay, C., Detournay, E., 2004. Self-excited stick-slip oscillations of drill bits. Compt. Rendus Mec. 332 (8), 619–626. https://doi.org/10.1016/j.crme.2004.01.016.

Richard, T., Germay, C., Detournay, E., 2007. A simplified model to explore the root cause of stick–slip vibrations in drilling systems with drag bits. J. Sound Vib. 305 (3), 432–456. https://doi.org/10.1016/j.jsv.2007.04.015.

Runia, D.J., Dwars, S., Stulemeijer, I.P.J.M., 2013. A brief history of the Shell "Soft Torque Rotary System" and some recent case studies. In: SPE/IADC Drilling Conference. Society of Petroleum Engineers, pp. 69–76. https://doi.org/10.2118/163548-MS.

Tobias, S.A., 1965. Machine Tool Vibration. Blakie, London.

Vromen, T., van de Wouw, N., Doris, A., Astrid, P., Nijmeijer, H., 2017a. Nonlinear output-feedback control of torsional vibrations in drilling systems. Int. J. Robust Nonlinear Control 18 (October 2014), 557–569. https://doi.org/10.1002/rnc.3759. arXiv:arXiv:1505.02595v1.

Vromen, T., Dai, C.-H., van de Wouw, N., Oomen, T., Astrid, P., Doris, A., Nijmeijer, H., 2017b. Mitigation of torsional vibrations in drilling systems: a robust control approach. IEEE Trans. Control Syst. Technol. 1–17. https://doi.org/10.1109/TCST.2017.2762645.

Wahi, P., Chatterjee, A., 2008. Self-interrupted regenerative metal cutting in turning. Int. J. Non-Linear Mech. 43 (2), 111–123. https://doi.org/10.1016/j.ijnonlinmec.2007.10.010.

Weatherford, 2010. Dailey R-A-M Shock Absorber.

van de Wouw, N., Vromen, T., Detournay, E., Nijmeijer, H., 2017. Delay system modelling and analysis of a down-hole tool in drilling systems. In: Stépán, G., Csernák, G. (Eds.), Proceedings of the 9th European Nonlinear Dynamics Conference. CongressLIne Ltd., Budapest.

Yigit, A.S., Christoforou, A.P., 2006. Stick-slip and bit-bounce interaction in oil-well drillstrings. J. Energy Resour. Technol. 128 (4), 268. https://doi.org/10.1115/1.2358141.

Zhang, L., Stepan, G., 2016. Exact stability chart of an elastic beam subjected to delayed feedback. J. Sound Vib. 367, 219–232. https://doi.org/10.1016/j.jsv.2016.01.002.